Russian Geology and Geophysics © 2019, V.S. Sobolev IGM, Siberian Branch of the RAS
Vol. 60, No. 3, pp. 338–356, 2019 DOI:10.15372/RGG2019020 *Geologiya i Geofizika*

Dynamics of the Seismic-Energy Structure on the Southwestern Flank of the Baikal Rift System: Andronov–Hopf Bifurcation

A.V. Klyuchevskii ✉, V.M. Dem'yanovich

Institute of the Earth's Crust, Siberian Branch of the Russian Academy of Sciences, ul. Lermontova 128, Irkutsk, Russia, 664033

Received 20 April 2017; received in revised form 16 April 2018; accepted 26 July 2018

Abstract—The dynamics of the seismic-energy structure state on the southwestern flank of the Baikal rift system (BRS) has been analyzed at three hierarchical levels based on the annual cumulative data on the earthquakes with energy class $K_R \geq 8$ for the period 1964–2013. Changes in the state are characterized by three key parameters: maximum energy class K_{max}, the slope of the earthquake recurrence curve γ, and seismic activity A_{10}. With an increase in the earthquake recurrence intervals and the quantity of the earthquakes analyzed, the parameters reach their maxima reflecting the regularity of earth shocks classification by long periods. Two attractors are clearly distinguished in the phase pattern, where they reflect general quasi-stationarity (limit cycle) and local instability (focus) of the seismic-energy structure. The specifics of the attractor formation suggest a cycle birth bifurcation (Andronov–Hopf bifurcation). For a detailed analysis of the dynamics of seismic-energy structure formation, the slopes of the earthquake recurrence rate curves were calculated in the simulation scenarios of "aftershocks" and "swarm" earth shocks. Comparison of the simulated and real changes in the earthquake recurrence rate slopes shows a correspondence of the "aftershock" model to the dynamics of the seismic-energy structure of the lithosphere on the BRS southwestern flank.

Keywords: Baikal rift system, southwestern flank, seismicity, energy structure, dynamics model, Andronov–Hopf bifurcation

INTRODUCTION

Monitoring of seismicity is an efficient tool used for studying seismotectonic processes, strong earthquakes prediction, general seismic zoning and verification of geodynamic and seismic models. So that, according to the seismic quiescence model, an increase in an average rate of the earthquake flow within the area of strong shock preparation (Keilis-Borok et al., 1988; Sykes and Jaume, 1990) will cause a decrease in the earthquake flow rate within the source zone (Wiemer and Wyss, 1994; Sobolev, 1999). A relation between variations in the velocity of the Earth's axial rotation and changes in a time span of seismic process intensity has been demonstrated in (Gor'kavyi et al., 1999). A study of the Baikal rift system (BRS) has shown that its epicentral region is divided into three areas (southwestern and southeastern flanks, and the BRS central part) (Klyuchevskii and Demyanovich, 2003); each area has a rifting attractor structures (RAS) (Klyuchevskii, 2011, 2014). Stress alternation in the BRS lithosphere tends to form synchronization episodes of the seismic flow rate (Klyuchevskii and Klyuchevskaya, 2009). Furthermore, strong paired earthquakes appear to be a consequence of the stress alternation (Klyuchevskii, 2010; Klyuchevskii and Khlebopros, 2013). The above-mentioned and many other findings indicate the dependence of seismicity and strong earthquakes on global, regional and local geodynamic events of different nature which lead to variations in the stress-strain and/or rheological medium state. To detect, identify, compare and explain these events and relations, we have to obtain reliable consistent data on the seismicity as a function of space, time and energy as well as proven, physics-based data processing and analysis techniques (Zav'yalov, 2006).

Earthquakes classification by the energy class scale allows us to determine earthquake recurrence parameters in order to compare the seismic-energy structure from different areas and to carry out the analysis of structure state variations in time. Earthquake recurrence graphs have long been used for studying seismic-energy and estimating an average recurrence rate of strong events. The slope of the recurrence curve γ depends on the strong—weak earthquakes ratio. The graph level characterizes seismic activity as A—the number of the earth tremors/shocks of fixed energy class being normalized on space and time bases, and K_{max} is energy class of the maximally possible earthquake in the investigated lithosphere zone. Parameters (γ, A and K_{max}) reflect in the integrated form elastic and rheological lithosphere properties and also the rate of its internal deformation increase (Gaiskii, 1970).

To classify seismic events of the Baikal Region, T.G. Rautian (1964) energy class scale labeled as K_R is used. Here for the whole period of instrumental observations, seismicity is conventionally characterized by earthquake recur-

✉ Corresponding author.
E-mail adress: akluchev@crust.irk.ru (A.V. Klyuchevskii)

rence curves applying this scale (Golenetskii, 1989; Golenetskii et al., 1993; Klyuchevskii, 2005, 2007; Klyuchevskii et al., 2015). For the scale of energy classes K_R the graph of the earthquake recurrence rate is represented as follows (Riznichenko, 1968):

$$\lg N = \lg A_{10} + \gamma (K_R - K_{R_0}) \text{ at } K_R \le K_{max}, \quad (1)$$

$$N = 0 \text{ at } K_P > K_{max},$$

where N denotes the number of seismic events, and K_{R_0} = 10—a fixed energy class. Being statistically calculated by sampled space-time referenced data, the complex of expressions (1) allows describing the state of the seismic-energy structure in the studied territory using the value—K_{max}, the slope of the earthquake recurrence rate curve γ and seismic activity—A_{10}. Accumulated seismological up-to-date information enables us to study, analyze and obtain a general estimator of the seismic-energy structure for the Baikal Region comprised of separate territories (Klyuchevskii et al., 2012). Here, the states of the seismic-energy structure on the southwestern flank of the BRS (φ = 49.0–54.0° N, λ = 96.0–104.0 °E) have been studied in three territories for the period of instrumental observations from 1964 to 2013. The main object characteristic is known to be its structure (Stepin, 2010), i.e., the set of stable relations which allows preservation of key properties under conditions of internal/external variations. A study of seismic-energy structure implies determination of a set of stable relations to distribute earthquakes on an energy class scale, which ensures identity and preservation of key properties on various spatial-time scales. Following this approach, using of the data sampled in different territories or various time periods enables us to study the dynamics and understand the specifics of the parameters definition for the earthquake recurrence rate graph (i.e., characteristics of the seismic-energy structure) on different hierarchical lithosphere levels. It also allows one to estimate the parameters accuracy, to find the reasons of deviations from the stable state, to compare experimental results with numerical ones and to refine a final model of seismic-energy structure dynamics.

MATERIALS AND METHODS

The general structural condition and the BRS contemporary dynamics are known (Logachev, 2003) to be determined by the relation with the suture zone of Precambrian Siberian Craton and the Central Asian mobile belt. The single rift "stem" combining the South Baikal and Tunka depressions is divided into the Busiingol, Darkhat and Hövsgöl depressions with a sudden change of the strike (from latitudinal to longitudinal) at the southwestern flank of the BRS. The large Bolnai shear appears to be a growth borderline for the rift faults and valleys to the south. In 1905, it was renewed by a strong earthquake over a length of 370 km with a left-side slip up to 6–8 m, so there are no typical rift valleys southwards of the Bolnai fault. The present study considers the BRS to be a separate element, whose current geodynamics and seismicity formation are predominantly affected by RAS in the area of Lake Hövsgöl (Klyuchevskii, 2011, 2014). Furthermore, its stress-strain state lithosphere is spatially nonuniform and unstable in time (Dozer, 1991; Klyuchevskii and Demyanovich, 2006; Klyuchevskii et al., 2009).

The original materials were taken from "Earthquakes Catalogue of the Baikal Region", containing general information on earthquakes in the region (Golenetskii et al., 1993). These catalogues have been prepared by the group members in charge of summary seismic data processing at the Baikal Department of the Federal Research Center of the Geophysical Survey, Russian Academy of Sciences (http://www.seis-bykl.ru). It should be noted, that since 2003 the materials of "The Earthquakes Catalogue of the Baikal Region" have been presented within new borders of seismically active Russia's regions and territories (Earthquakes…, 2007, 2010), where the western borderline of the Baikal Region is displaced from the longitude λ = 96.0° to λ = 99.0° E. The paper presents the analysis of changes in the state of the seismic-energy structure of the following lithosphere zones (Fig. 1): (1) the southwestern flank of the BRS (region); (2) two areas formed through division of the region territory into halves by the longitude λ = 100.0°, and area numbers (1, 2) are indicated from the west; (3) two fault zones with the length L and the width $W = \pm 30$ km from the fault axis (Klyuchevskii and Demyanovich, 2004; Demyanovich et al., 2008): the Belino-Busiingol zone (BB—fault, area 1, L = 202 km), the Tunka zone (Tk—fault, area 2, L = 146 km). These geological areas could be considered as three consecutive hierarchical levels of lithosphere nonhomogeneities (Sadovskii, 1979). For detailed studies, the territory of the southwestern flank was divided into 1° × 1° sites, which sizes approximately correspond to the third (fault) hierarchical level. We could also mention that the averaged shock density over the whole territory is equal to about 280 events per square degree. Earthquake recurrence curves on 1° × 1° sites will be determined if the number of the earthquakes (happened during 1964–2013) amounts to $N \ge 13$. It is a minimal quantity of shocks needed to form the first "equilibrium" state for the first three energy classes of the sampling ($n_8 = 9$, $n_9 = 3$, $n_{10} = 1$, $\gamma_p \approx -0.477$, correlation coefficient $\rho \approx 1.0$, see below).

The slopes of earthquake recurrence curves γ and g were calculated by the root mean square (RMS, γ) and by the method of maximum likelihood (MML, g) for annual and cumulative sampled data on earthquakes from all the territories over the period of 1964–2013. The MML is recommended for g determination when the number of sampled earthquakes is not higher than 1000 events (Zhalkovskii and Muchnaya, 1987), that is frequently realized in the present study. The results of the numerical modeling of the earthquakes sequences (Demyanovich and Klyuchevskii, 2013) agree well with the conclusions made by N.D. Zhalkovskii

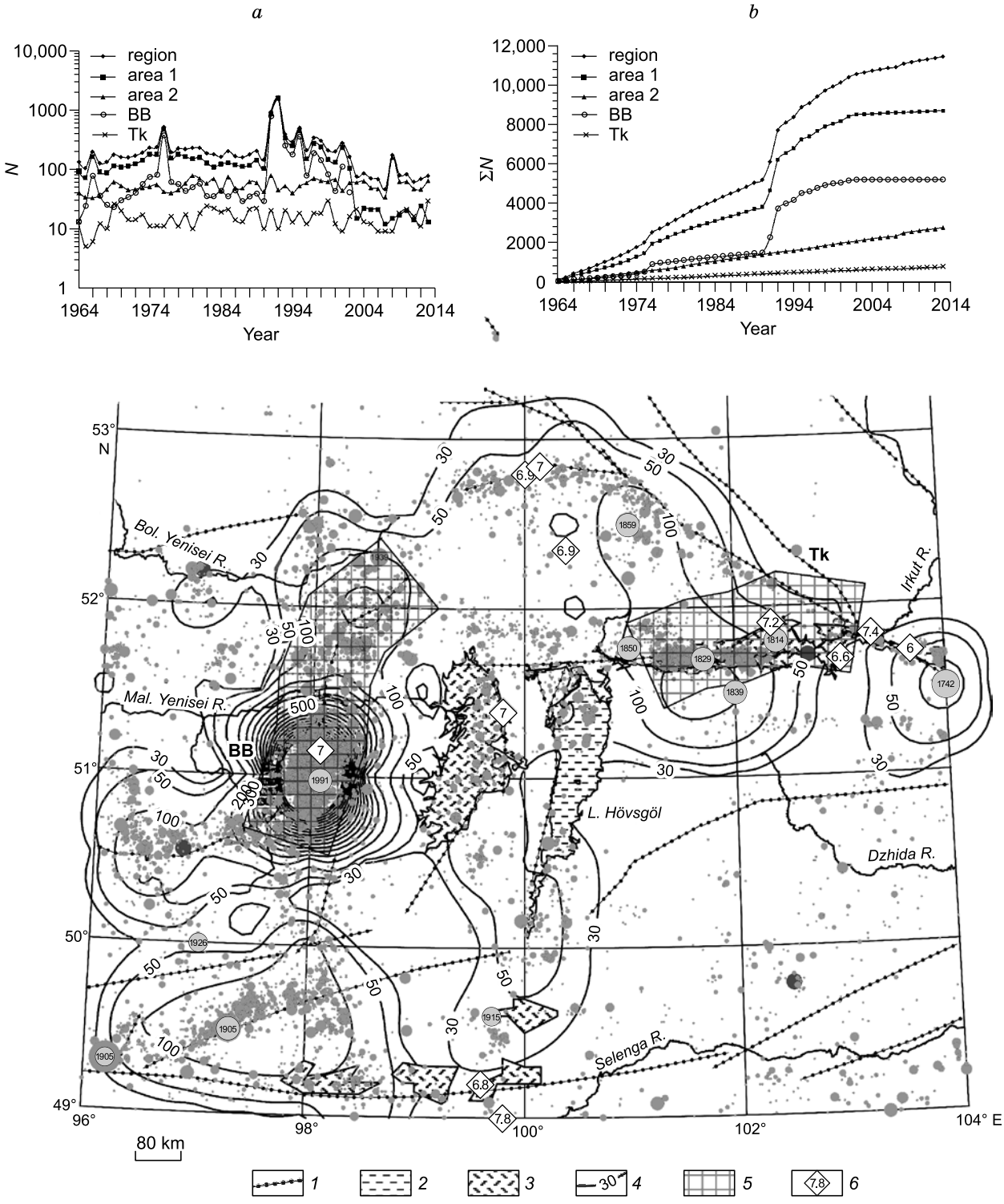

Fig. 1. Contour map of earthquake epicenters on the southwestern flank of the Baikal rift system and isolines of earthquake distribution density on 0.5° × 0.5° sites. The curves of the annual (*a*) and accumulated summarized over years' time intervals (*b*) earthquake numbers in the investigated territories. *1*, main faults, *2*, lakes, *3*, depressions, *4*, isolines of earthquake epicenters distribution density, *5*, zones of the Belino-Busiingol (BB) and Tunka (Tk) faults, *6*, paleoquakes with $M \geq 6$ and at the age of up to two thousand years (Klyuchevskii et al., 2013), *7*, earthquake epicenters with energy class $K_R \geq 8$ (1964–2013), *8*, earthquake epicenters of the historical and instrumental period (1740–2013) with $M \geq 6$.

and V.I. Muchnaya (1987) and show that MML estimates are more stable and, consequently, more preferable for characteristics of the long-term seismic-energy structure. The stability of RMS estimates tends to grow with an increase in data volume, and their high dependence on variations in shocks distributions makes the method more suitable for studying the dynamics of the seismic-energy structure. MML and RMS estimates tend to converge with an increase in samples volume. Calculations of seismic activity (A_{10}) were done by the formula (Golenetskii, 1981), which differs from the known Yu.V. Riznichenko (1964) formula by the multiplier in square bracket and allows making A_{10} more precise for shocks samples within a small range of energy classes:

$$A_{10} = 1000 \times N(1–10^{-\gamma}) / \{10^{-\gamma\,(K\min–10)} \times [1–10^{-\gamma\,(K\max–K\min+\,1)}] \times S \times T\}. \quad (2)$$

Here, N is the number of shocks, γ, the slope of the earthquake recurrence rate curve, K_{min} and K_{max}, maximum and minimum energy classes of shocks per site, S, km^2, an area, T = 50, observations period.

RESULTS

Hundreds of underground shocks with different energy are annually recorded in the lithosphere of the southwestern BRS flank. At the beginning of the 20th century the most disastrous Tsetserleg (09.07.1905, φ = 49.5° N, λ = 97.3° E, M = 7.6, K = 17) and Bolnai (23.07.1905, φ = 49.3° N, λ = 96.2° E, M = 8.2, K = 18) earthquakes took place. Figure 1 presents a contour map of epicenters and isolines of earthquakes distribution density on the southwestern BRS flank with energy class $K_R \geq 8$. Here the data of instrumental observations are represented for the period of 1964–2013, when quite closely spaced shocks with $K_R \geq 8$ were recorded (Golenetsky, 1990). Hence shown on the map, the scattered field of earthquake epicenters represents the latitudinal-longitudinal distribution of the main faults, which is affected by rift stem division and characterized by the maximal Hausdorff fractal dimensionality D_0 in the Baikal Region, mainly D_0 = 1.60 (Klyuchevskii and Zuev, 2007). Figure 1 shows that epicenter distribution maxima are formed by aftershocks of two Busiingol earthquakes in the west (01.04.1976, K_R = 14, φ = 51.15° N, λ = 97.97° E; 27.12.1991, M_{LH} = 6.5, K_R = 16.2, φ = 50.98° N, λ = 98.08° E), but in the south they are formed by earthquakes in the zone of Tsetserleg and Bolnai faults, and in the northeast—by shocks within the Tunka fault zone and the western area of the Kultuk earthquake aftershocks (27.08.2008, M_S = 6.1, K_R = 15.9, φ = 51.62° N, λ = 104.06° E). The zones of shocks concentration usually correspond to epicenters of strong earthquakes and paleoquakes. The isoline with N = 30 separates seismicity of the southwestern flank from the epicenter field of the central BRS part, the Altai–Sayan Region and southern Mongolia to highlight the relative "independence" of this lithosphere part.

Figure 1*a* presents graphs of annual earthquake numbers (*N)* in the investigated territories, where N tends to fluctuate. The most noticeable increases in shock flow rates were caused by the Busiingol earthquake aftershocks in 1976 and 1991–1992, while in 2008 the maximum was reached due to the aftershocks of the Kultuk earthquake. The minimum quantity of annual earthquakes (N_{min} = 5) was observed within the Tk-fault zone in 1965, and the maximum (N_{max} = 1600) is labeled on the district curve in 1992. In 2003 a considerable reduction in the earthquake flow rate is also seen over the region and the first area, and the shock number equals 0 in the BB-fault zone. These changes reflect the consequences of the western Baikal Region border transition from the longitude λ = 96.0° to λ = 99.0° E. According to the earthquakes Catalogue of the Baikal Region, shocks have not been observed to the west of λ = 99.0° E since 2003. In Fig. 1*b* you can see the curves of cumulated and annually summarized shock figures ΣN, which significant changes were caused by the Busiingol earthquake aftershocks in 1976 and 1991–1992. Minimal earthquake quan-

Table 1. Parameters of earthquake recurrence curves and distribution of the earthquake numbers over energy class K_R in different territories on the southwestern flank of the Baikal rift system for the 1964–2013

Territory	K_R									The total number of shocks	γ	±Δγ	g	A_{10}	K_{max}	K^{Cat}_{max}
	8	9	10	11	12	13	14	15	16							
R	7784	2531	750	241	92	34	9	0	1	11,442	–0.51	0.02	–0.49	0.05	16.2	18
A1	5951	1921	555	169	65	26	5	0	1	8693	–0.50	0.02	–0.50	0.08	16.2	18
A2	1847	613	198	72	27	8	4	0	0	2769	–0.45	0.01	–0.47	0.03	14.4	17
BB	3604	1131	310	97	32	16	2	0	1	5193	–0.48	0.02	–0.51	0.64	16.2	16.2
Tk	513	181	54	13	7	1	2	0	0	771	–0.45	0.03	–0.48	0.14	14.0	16
Average and standard deviation on the territories											–0.48 ± 0.02	0.02 ± 0.01	–0.49 ± 0.01			

Note. R, region, southwestern flank of the Baikal rift system; A1 and A2, area 1 and 2; BB and Tk, zones of the Belino-Busiingol and Tunka faults; γ and ±Δγ, the slope of earthquake recurrence rate curve and its standard deviation (RMS); g, the slope of earthquake recurrence rate curve (MML); A_{10}, seismic territorial activity; K_{max}, maximum energy class against data of instrumental observations in this territory from 1964 to 2013; K^{Cat}_{max}, maximum energy class designated in the earthquakes Catalogue of the Baikal Region on the territory from 1740.

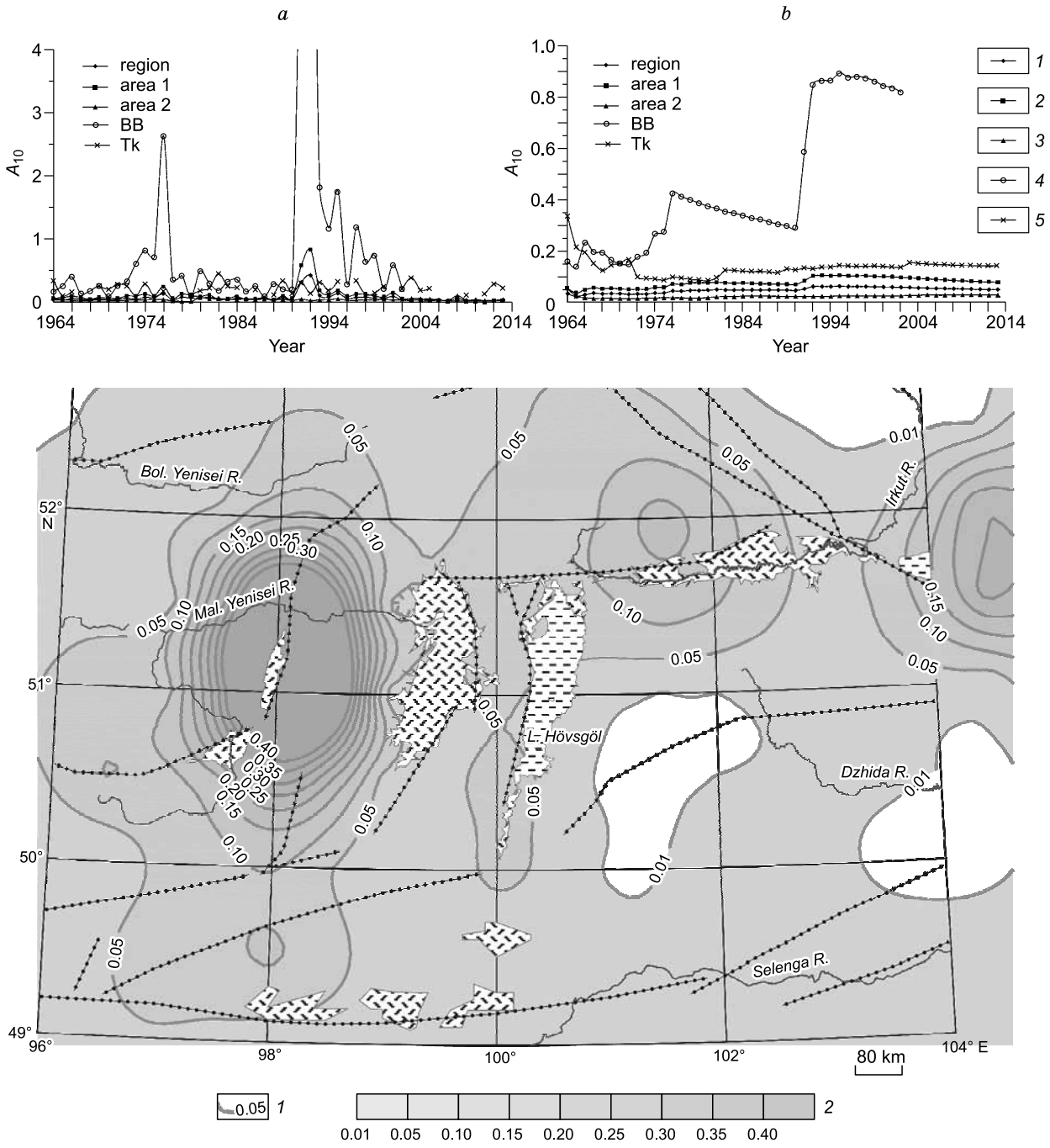

Fig. 2. Contour map of seismic activity A_{10} in the territory of the BRS southwestern flank plotted against the data on earthquakes (with $K_R \geq 8$) recorded for the period of 1964–2013 on 1° × 1° sites. The curves of the parameter A_{10}, obtained by annual (*a*) and accumulated (*b*) earthquake samples in the investigated territories. *1*, isolines of the parameter A_{10}, *2*, the isoline scale of the parameter A_{10}. See Fig. 1 for other designations.

tity (ΣN_{min} = 13) is marked on the Tk-fault zone curve in 1964, and the regional maximum (ΣN_{max} = 11,442) is indicated on the curve in 2013.

Table 1 provides a distribution of the earthquake numbers by K_R and recurrence graphs parameters of the investigated territories over the period of 1964–2013. According to Table 1, fault zones are characterized by high values of γ and A_{10}, that points at weight dominance of strong earthquakes over weak shocks, so strong shocks tend to happen within a zone of a large fault, but weak shocks are scattered over the regional territory and caused by a network of small and active faults. The minimal slope of $\gamma \approx -0.51 \pm 0.02$ corresponds to the district, but the maximal one $\gamma \approx -0.45 \pm 0.03$ fits for the Tk-fault zone. Higher seismic activity is observed

in the BB-fault zone, but the lowest one ($A_{10} \approx 0.03$) is seen in the second area. According to historic data given in the earthquakes Catalogue of the Baikal Region (record from 1740), the disastrous Bolnai earthquake with $K^{Cat}_{max} = 18$ happened on the southwestern BRS flank in 1905, and several strongest earthquakes with $K^{Cat}_{max} = 17$ were recorded in given time. The strong Busiingol earthquake was recorded on 27.12.1991 with $K_{max} = 16.2$. The magnitude of the strongest paleoquake reaches $M_{max} \approx 7.8$ (the Bolnai fault zone, Dzuunnuur seismic dislocation, φ = 49.0° N, λ = 99.8° E, age 300–500 years) (Dzhurik et al., 2009).

A_{10} and K_{max} were calculated by sampled data on earthquakes with $N \geq 13$ on 1° × 1° sites; smoothing was done by the site displacement at 0.5° of the latitude and longitude

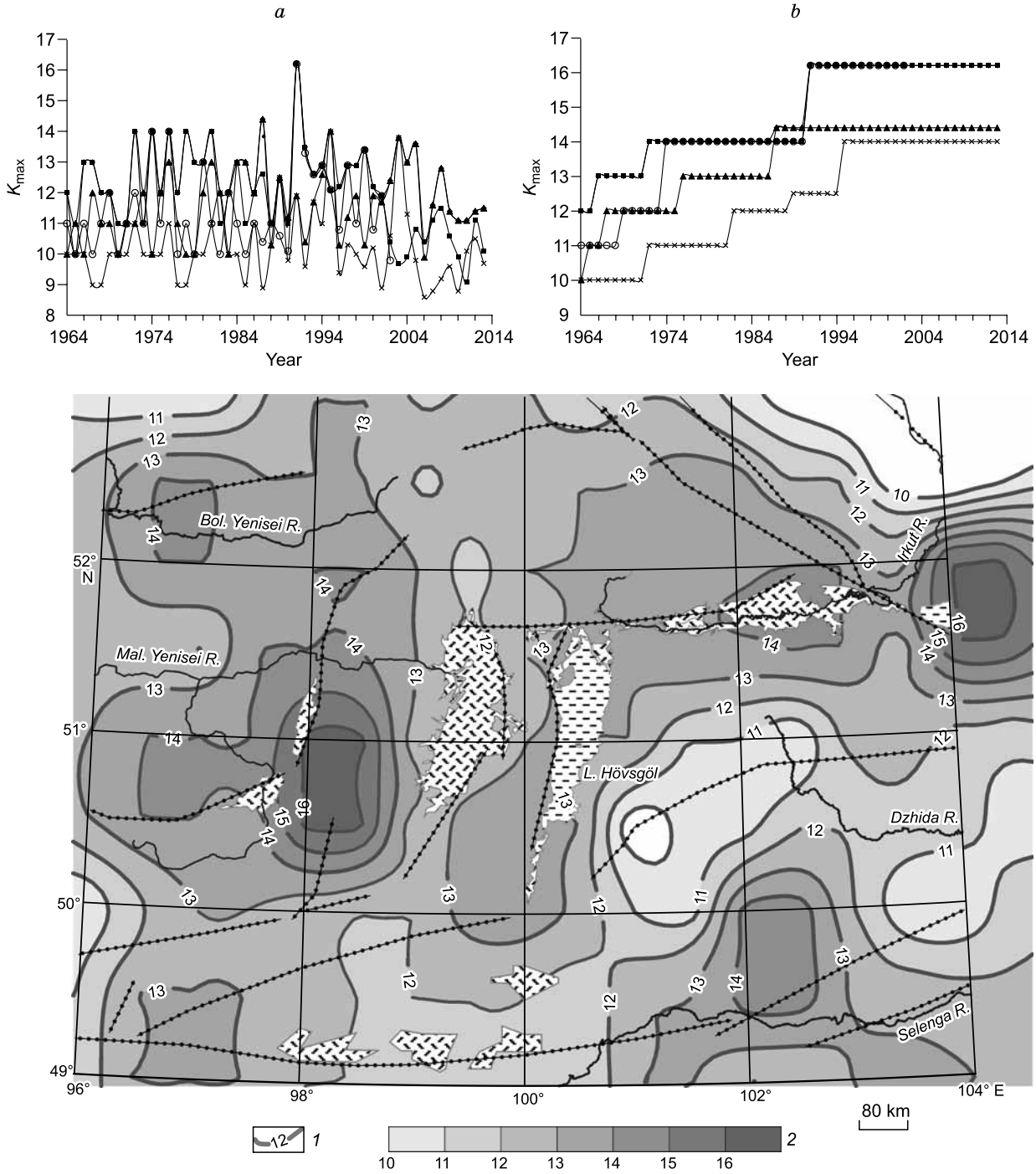

Fig. 3. Contour map of maximum energy class K_{max} on the territory of the BRS southwestern flank constructed against the data on earthquakes with $K_R \geq 8$, which were recorded on 1° × 1° sites over the period of 1964–2013. The curves of the parameter K_{max}, plotted against annual (*a*) and accumulated (*b*) earthquake samples on the investigated territories. *1*, isolines of the parameter K_{max}, *2*, the isoline scale of the parameter K_{max}. See Fig. 1 for other designations.

(the contour maps with γ and *g* parameters were obtained in the same way. The map-diagram (Fig. 2) of seismic activity A_{10} was plotted in accord with the data on earthquakes recorded for the period of 1964–2013 on 1° × 1° sites. Nearly all the territory of the southwestern flank is covered by the isoline $A_{10} = 0.01$. Three areas of higher activity are clearly distinguished, such as the aftershock area of the Busiingol earthquakes ($A_{10} \approx 0.89$), the Tk-fault zone ($A_{10} \approx 0.18$) and the aftershock area of the Kultuk earthquakes ($A_{10} \approx 0.27$) in the east. There exist two zones of lower activity to the east of Lake Hövsgöl. The curves of annual A_{10} values vary within notable limits (Fig. 2*a*): peaks of maximum activity are observed in the BB-fault zone in 1976 ($A_{10} \approx 2.63$), in 1991 ($A_{10} \approx 6.85$) and in 1992 ($A_{10} \approx 9.63$); minimum activity ($A_{10} \approx 0.01$) was detected in the second area in 1978. Variations in A_{10} curves on the accumulated seismicity are less significant: from $A_{10} \approx 0.01$ in the second area in 1970 to $A_{10} \approx 0.89$ within the BB-fault zone in 1995 (Fig. 2*b*). It should be noted that A_{10} varies slightly within the time both in the region and the areas, but a dramatic rise of activity is recorded in the BB-fault zone owing to the impact of the strong earthquakes in 1976 and 1991 and their aftershocks, and then the peak is followed by a gradual fall of activity.

It is difficult to estimate energy class K_{max} of the maximally feasible earthquake in the lithosphere on the southwestern flank of the BRS by the available instrumental materials. Within the determination error limit, the magnitude of the Bolnai earthquake (in 1905; $M = 8.2$) corresponds to the magnitude ($M_{max} \approx 8.5$) of the maximally feasible earthquake in the Baikal Region (Ruzhich et al., 1998). Figure 3 shows a contour map of maximal energy classes of the earthquakes, which took place on the 1° × 1° sites over the period from 1964 to 2013. The isoline ($K_{max} = 16$) delineates the Busiingol earthquake (1991) zone and the zone of the Kultuk earthquake (2008) on the map; several areas with $K_{max} = 14$ are also seen. Almost all the territory is covered with the isoline ($K_{max} = 12$), and the only site with $K_{max} = 10$ is found to the west from Lake Hövsgöl. The curves of annual values tend to vary from $K_{max} = 9$ within the Tunka fault zone up to $K_{max} = 16.2$ in 1991 on the three territories (Fig. 3*a*). Variations in the curves of the accumulated seismicity are also considerable—from $K_{max} = 10$ in the Tunka fault zone to $K_{max} = 16.2$ on the three territories; the trend of K_{max} growth within the time is being observed on all the territories (Fig. 3*b*). It should be mentioned that the contour map and curves (Fig. 3) reflect the main features of the spatial-time distribution of the seismic energy $E \approx 10^{K_{max}}$.

Figure 4*a* represents annual estimates obtained from the slopes of the earthquake recurrence curves, where the values vary from $\gamma = -0.15$ in the Tk-fault zone (1964) to $\gamma = -0.80$ in the second area (1979). Changes in *g* are less significant—from $g = -0.26$ (2003) to $g = -0.76$ (1973) within the Tk-fault zone (Fig. 4*b*). It should be mentioned that variations in γ and *g* are getting greater with a decrease in the territory sizes when taking maximum values for small samples of earthquakes in the Tk-fault zone. The curves (Fig. 5) constructed using cumulative sampled data demonstrate absolutely different behavior. The slopes of the earthquake recurrence curves differentiate significantly for the first ten years (from $\gamma = -0.15$ in the Tk-fault zone in 1964 to $\gamma = -0.58$ in the second area in 1972, from $g = -0.34$ in the Tk-fault zone in 1964 to $g = -0.50$ in the BB-fault zone in 1966); within the time they approach γ and *g* regional values. In 2013 we find the coincidence between the slopes of the earthquake recurrence curves for all the territories within the limits of standard deviation. In the early 1980s, a slight gradual decrease in γ and *g* is observed both in the region and areas within the time. The abrupt "jump" in γ and *g* values occurs in the BB-fault zone (1991) as a result of the strong Busiingol earthquake, and a less significant variation in the curve slope is specified by the earthquake recorded in 2003 (17.09.2003, $K_R = 13.8$, φ = 51.75° N, λ = 101.53° E). The trend (Fig. 5) towards smoothing and stabilizing the slopes of earthquake recurrence curves is relevant to summarized seismicity (Zav'yalov, 2006). It indicates that the slopes of earthquake recurrence rate curves commonly tend to approach extreme values with an increase in areas and/or in observation intervals, and generally with a rise in the number (*N*) of earthquakes for the sample available.

Figures 6 and 7 represent contour maps of γ and *g* parameters on the southwestern flank of the BRS. The bar chart represents the distribution of sites quantities (*n*) depending on the number of shocks (*N*) per site (Fig. 6*a*); it illustrates that not more than 400 events have happened on the most sites. *N* exceeds one thousand events on seven sites, and the ground shaking reaches its maximum ($N = 4749$ shocks) in the aftershock zone of the Busiingol earthquakes. Note that isolines γ, $g \geq -0.40$ along the exterior outline appear to be an extrapolation result and nearly all the territory with shocks density ($N \geq 30$) lies in the range of $-0.55 \leq (\gamma, g) \leq -0.45$. Maps comparison shows that the distribution pattern is the same for γ and *g* in the area, and the contour map for *g* parameter is less differentiated, and *g* value is less than the value of γ by about 0.05 (Figs. 6*b* and 7, insert). The slopes of earthquake recurrence curves on 1° × 1° sites tend to vary within the ranges: $-0.63 \leq \gamma \leq -0.19$ and $-0.84 \leq g \leq -0.35$; and the bar charts acquire the form close to normal distribution with an average value and standard deviation, where $\gamma = -0.42 \pm 0.09$ and $g = -0.48 \pm 0.07$ (Fig. 6*b* and 7, insert). The variance of slopes might be explained by inferior data representation, so the quantity of shocks does not exceed a hundred on 100 sites. The territory located eastwards from Lake Hövsgöl is distinguished by significant variations, where the maximum and minimum values of γ and *g* are determined on the adjacent sites at low density of shocks (Fig. 1).

Since the used spatial-time samples of earthquakes differ by volume, we can analyze the relationship of γ and its standard deviation σ with the quantity of shocks *N* in the samples. Based on annual and summarized information, a total

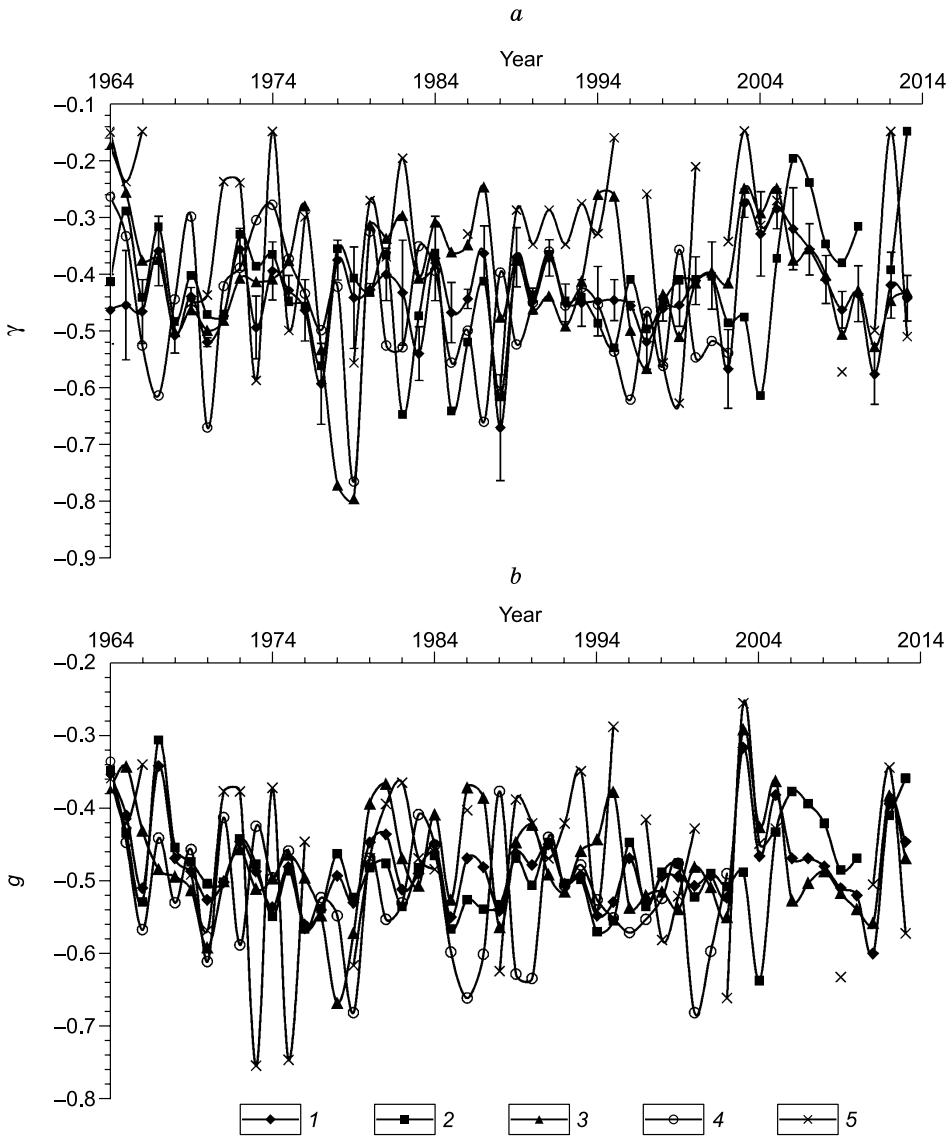

Fig. 4. The slopes of γ(*a*) and *g*(*b*) earthquake recurrence curves versus annual shock samples in the investigated territories. *1*, region, *2*, area 1, *3*, area 2, *4*, BB-fault, *5*, Tk-fault.

time sample was obtained, where the bar chart of samples quantities (*n*) distribution with the number of shocks (*N*) in them, takes the following form (Fig. 8*a*). In a few samples, *N* is higher than 10,000 although in most cases $N < 1000$. The distribution of *n* numbers over γ parameter approaches the normal one with an average value and standard deviation $\gamma = -0.45 \pm 0.09$ (Fig. 8*b*). Figure 8*c* represents distribution of γ versus *N* for the total time sample of materials. Significant variation of γ is seen in small data volumes—$N < 1000$. However, scattering tends to reduce with an increase of *N*. The graph (Fig. 8*d*) characterizes the relationship of standard deviation σ for γ determination with the sample volume (*N)* in the form of power-law dependence: $\sigma \approx 0.12N^{-0.22}$ with correlation index $\rho \approx 0.57$. We can see that σ tends to increase mostly for $N < 1000$. However, the presence of low σ for small-scale data samples points at the fact that the "right" (with regard to the indicating lg*N* values of each K_R on the earthquake recurrence curve or in proximity to it) distribution of a small sample lg*N* over K_R could result in low σ. Note that for the total sampling of area data, standard deviation over γ determination tends to decrease with the increase of *N* in the form of power-law dependence: $\sigma \approx 0.13N^{-0.22}$ with correlation index $\rho \approx 0.53$ and the number of samples $N = 182$. This equation is consistent with the estimates obtained over the total time data sample ($\sigma \approx 0.12N^{-0.22}$ with $\rho \approx 0.57$, $N = 470$ (Fig. 8*d*)); that could point at ergodicity of the dynamic system of seismogenesis.

To characterize the relationship of σ and γ, Fig. 9 represents correlation curves over 470 data samples in time (Fig. 9*a*) and 182 space/area samples (Fig. 9*b*). In both cases σ does not depend on the value of γ, because maximal and minimal values of σ are both observed within the whole

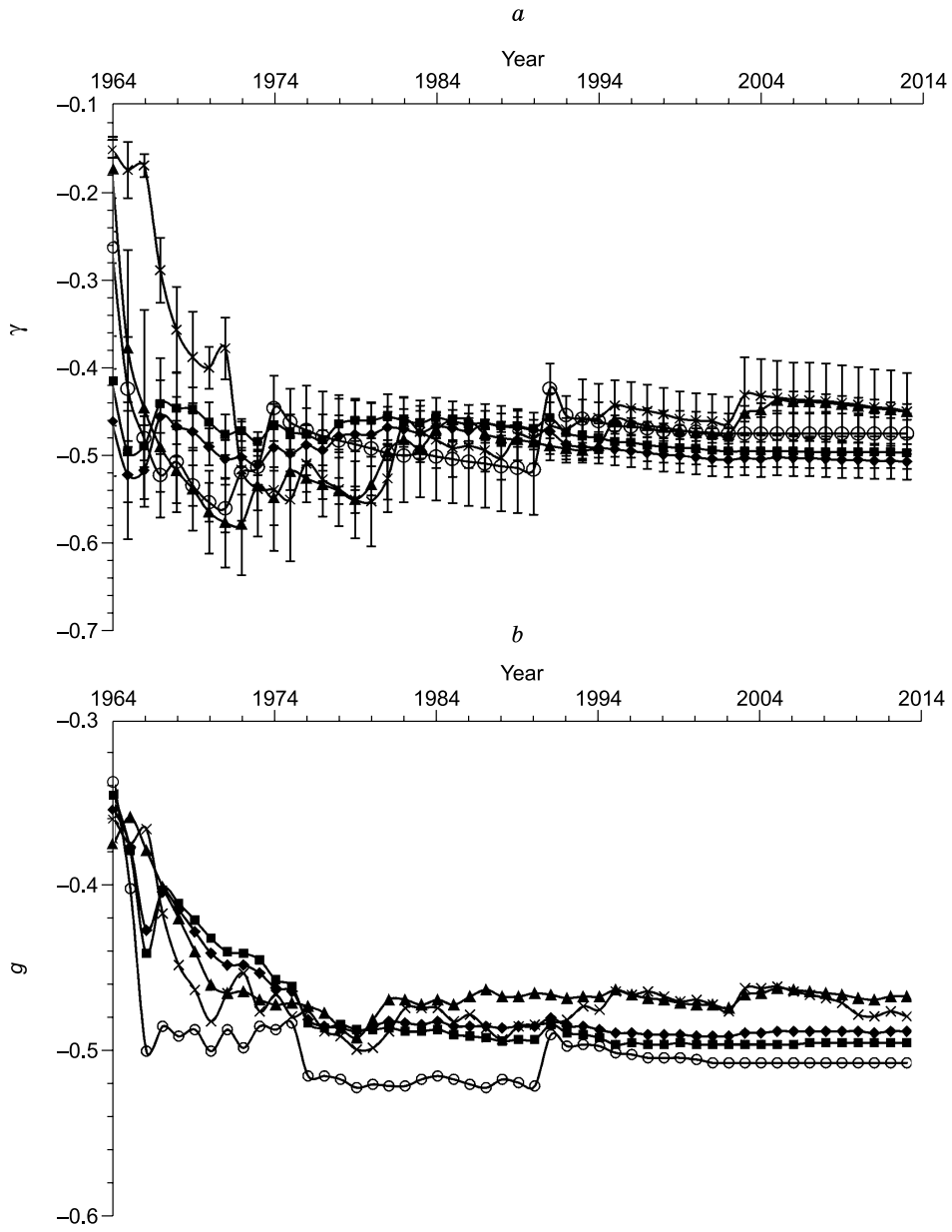

Fig. 5. The slopes of γ(*a*) and *g*(*b*) earthquake recurrence curves versus accumulated shock samples in the investigated territories. See Fig. 4 for other designations.

range of γ variations. Moreover, correlation and proportionality coefficients are low. Consequently, high and low values of γ sometimes can be determined with minor standard deviations for the "right" lg*N* distribution over K_R even for a small amount of ground shaking. In this case, standard deviation can't be a measure of γ-parameter validity.

Comparison of Figs. 2 and 3 illustrates that maximum or high seismic activity is observed in those places where the strongest earthquake and aftershock series are realized, but minimum seismic activity conforms to the absence of quite strong earth shocks. The relation analysis of γ with the number of shocks (*N*) and the value of maximum energy class (K_{max}) on 1° × 1° sites reveals the significant scattering of γ for samples with $N < 1000$ (Fig. 10*a, b*). The variance of γ tends to reduce with the increase of data volume. The presence of sampled strong earthquakes with $K_{max} \geq 13$ results in a rise of γ. Figure 10 shows that the upper contour of γ-values is represented only by such data samples; moreover, strong earthquakes will have greater effect on γ estimation and the slope will increase with a decrease in the sample volume. The equation of correlation relationship for the slope of the earthquake recurrence curve and maximum energy class of the sampled earthquakes will take the following form: $\gamma \approx -0.621 + 0.016K_{max}$.

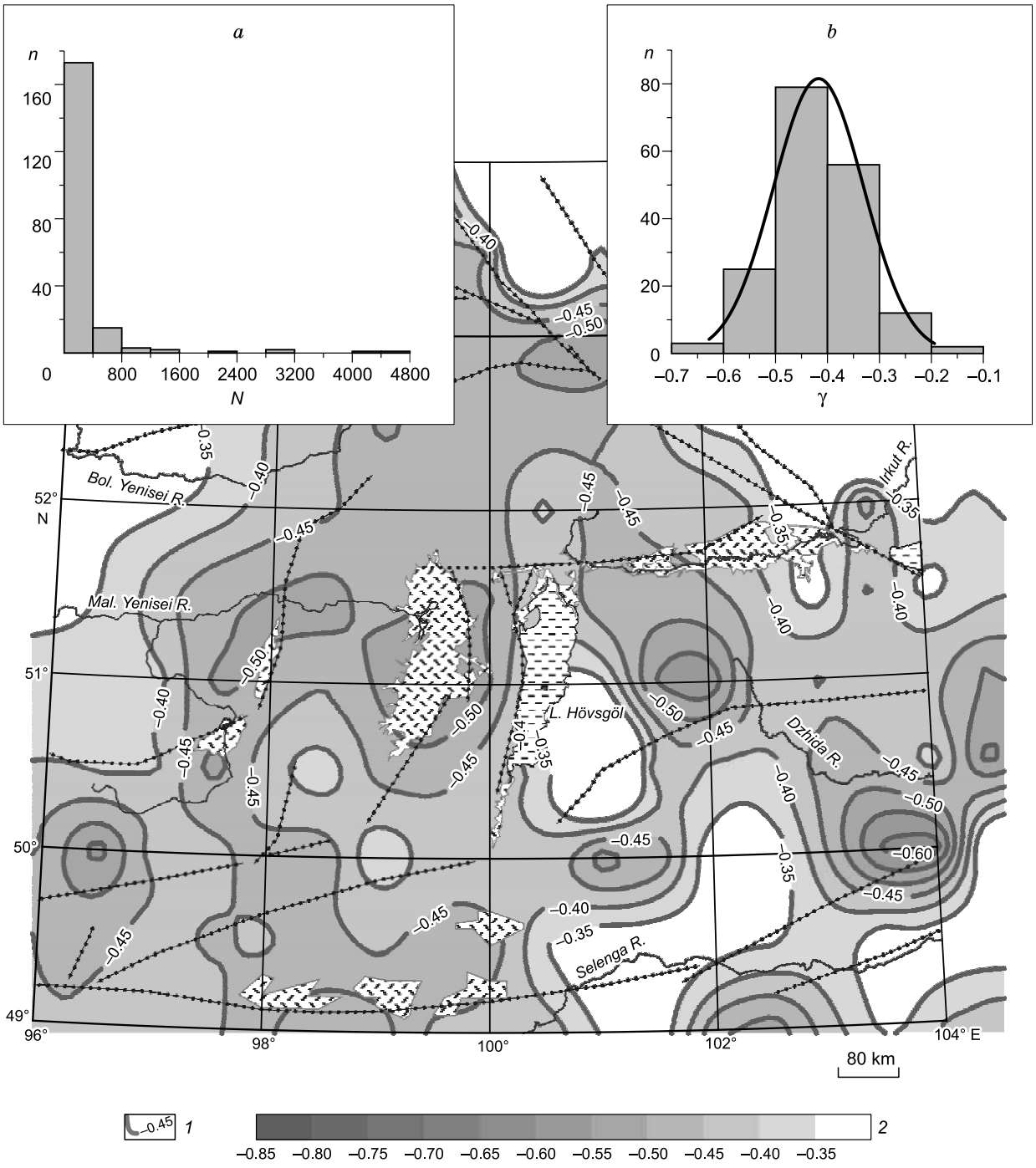

Fig. 6. Contour map with the slope of γ earthquake recurrence curve on the southwestern flank Baikal rift system constructed against the data on shocks with $K_R \geq 8$ recorded on 1° × 1° sites from 1964 to 2013. The bar chart of the sites quantities (*n*) distribution depending on the number of shocks (*N*) per site (*a*) the bar chart of γ distribution (*b*). *1*, isolines of the parameter γ, *2*, the isoline scale of the parameter γ. See Fig. 3 for other designations

DYNAMICS MODEL OF SEISMIC-ENERGY STRUCTURE

The variable systems (Prigozhin and Stengers, 1985) are known to be identified as dynamic, provided that physically it is a model of matter motion/displacement in the force field, but mathematically it is an operator functioning in space of states (phase space). The system states form a vector $\mathbf{x} = (x_1, x_2, \ldots, x_n)$ and are the axes of this space, and relate to the observed quantitative characteristics of the system. According to the theory of dynamic systems, a change in the vector state is defined by the vector field of velocities

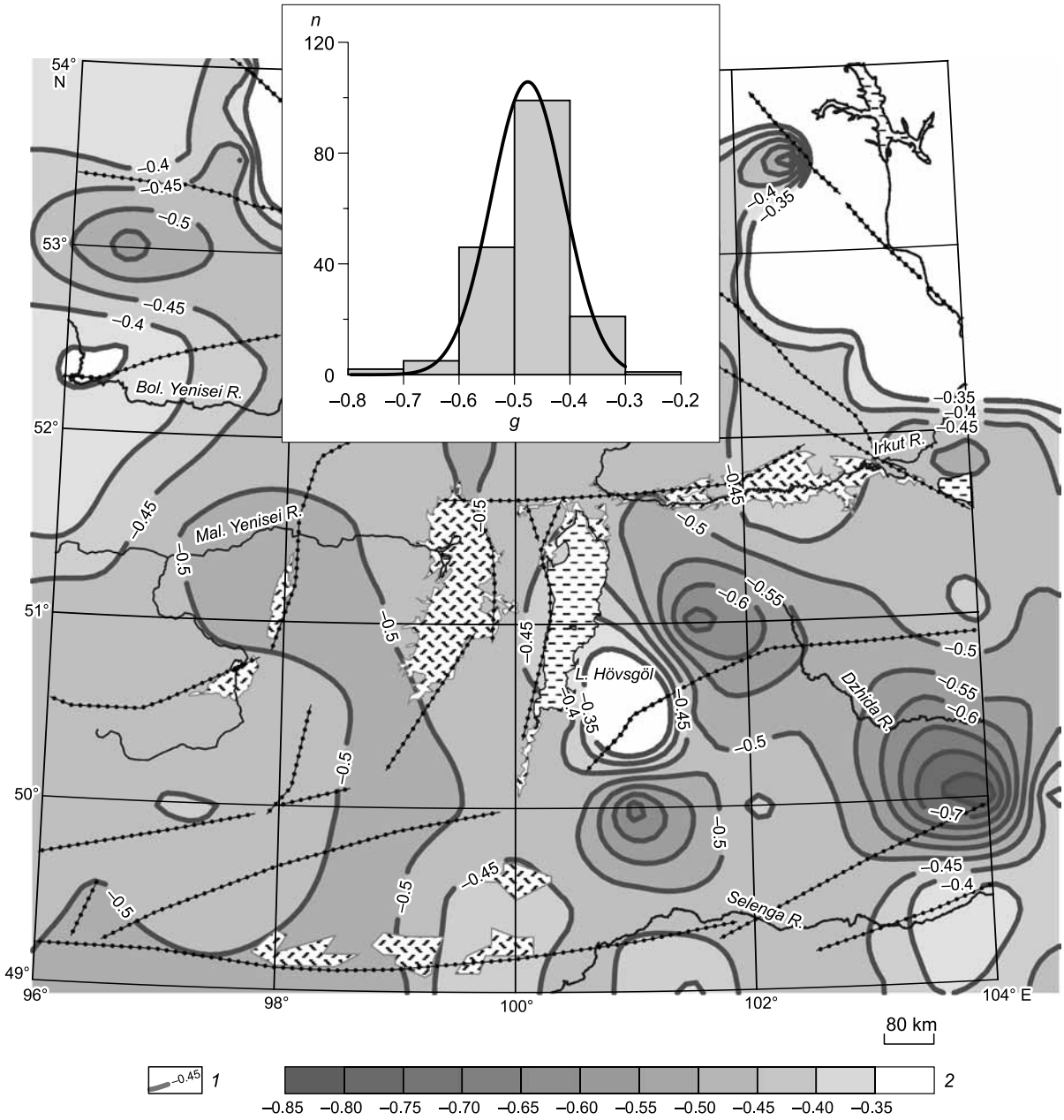

Fig. 7. Contour map with the slope of *g* earthquake recurrence curve across the southwestern flank Baikal rift system plotted against the data on shocks with $K_R \geq 8$ recorded on 1°×1° sites over the period of 1964–2013. The bar chart of *g* distribution. *1*, isolines of the parameter *g*, *2*, the isoline scale of the parameter *g*. See Fig. 1 for other designations.

$\mathbf{f}(\mathbf{x}(t))$, which appears to be an operator of the evolution system (Malinetskii and Potapov, 2000; Nikolis and Prigozhin, 2003). Such a dynamics model corresponds to the differential equation:

$$\frac{d}{dt}\mathbf{x} = \mathbf{f}\left(\mathbf{x}(t), \alpha\right), \tag{3}$$

where α denotes a control parameter. On condition that time changes discretely, the dynamics will be described by the Poincare mapping as:

$$x_{k+1} = F(x_k), \; k = 0, 1, 2, \ldots, \tag{4}$$

which may be either a result of equation (3) approximation or Poincare mapping or the only possible model of dynamics, in case the states are to be fixed only in isolated moments of time: k = 0, 1, 2, … The discrete maps of the dynamic system can be represented by law by connecting sequential points of the phase trajectory. The maps must be produced by the flow, and they are often used as the only technique to study structures and dynamics of natural systems.

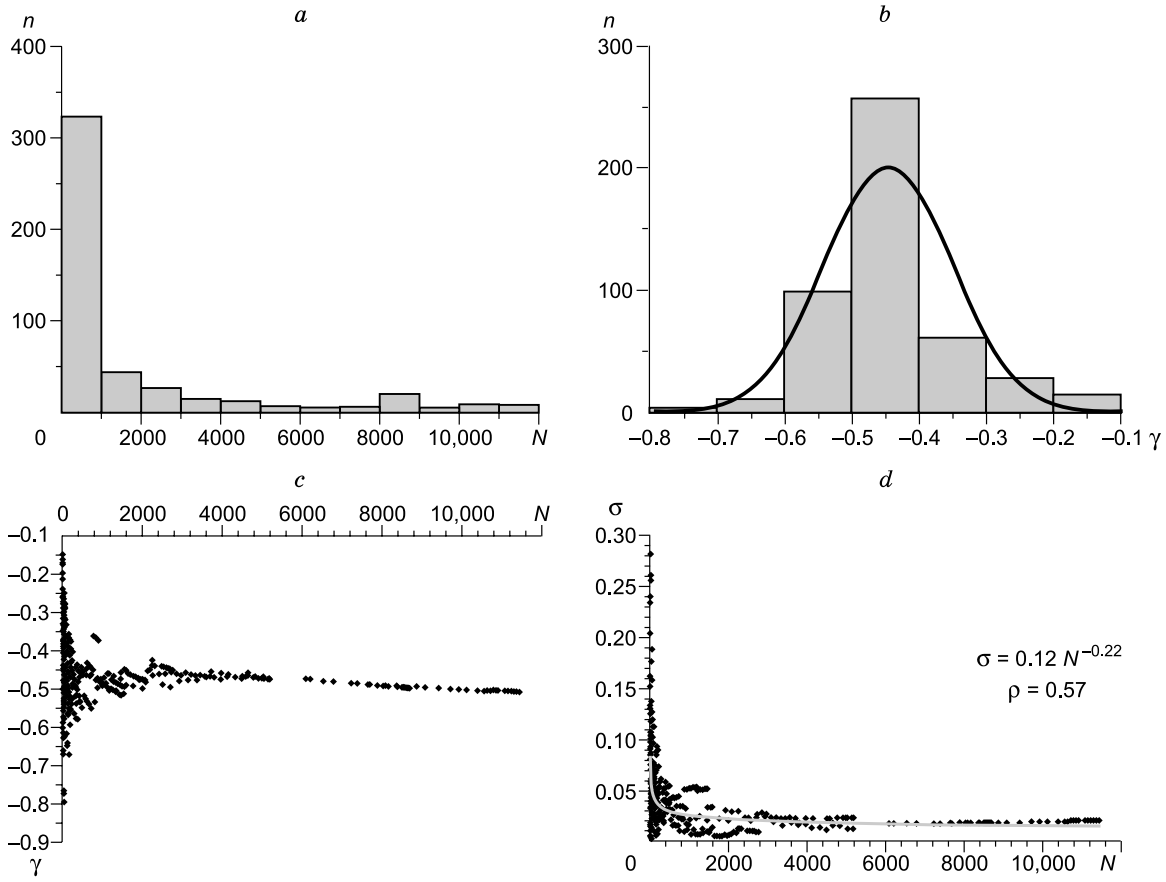

Fig. 8. The relation of γ parameter and its standard deviation σ with the quantity of shocks *N* over the "total" time sample. *a*, the bar chart of samples quantities (*n*) distribution with the number of shocks in the samples (*N*); *b,* the bar chart of γ distribution; *c,* distribution of γ versus *N*, *d,* the relation of standard deviation σ with the sample volume (*N).*

As shown in the study, the main variations in the state of the seismic-energy structure take place due to the occurrence of earthquakes with maximum energy class within a certain period of time. Since the earthquakes exceeding maximum-permissible energy class (or magnitude) cannot happen in the lithosphere (see formula (1)), jump-like variations in parameters on the earthquake recurrence curve (typical for these earthquakes realization) will tend to decrease with an increase in volume of sampled data within the time. In case the data samples are too large, the jumps in data are unlikely to find proper reflection in parameters variations on the earthquake recurrence curve. Consequently, we will probably have to change scales and a presentation form of energy structure state parameters, and switch to phase diagrams. This suggests that the use of a phase portrait for representation of energy structure dynamics could enable us to assign a stable attractor whose type and parameters are still unknown (limiting cycle, according to (Riznichenko and Artamonov, 1975)). However, the trend to forming the attractor is clearly traced on the graphs (Fig. 5). To illustrate the specifics of dynamics formation of the seismic-energy structure, a phase diagram of γ parameter for summarized regional earthquakes is given in Fig. 11 with 10-year intervals. With an increase in volume of the used data, the γ parameter is noticed to approach the attractor characterizing regularities in long-time shocks distribution on the available scale for estimation the earthquake size, whose basin is delineated with a small circle and labeled as "2013" ($\gamma \approx -0.505 \pm 0.02$). Trajectory contraction reflects a dissipative energy character of the dynamic seismogenesis and indicates that the relationship between the numbers of shocks of different energy classes becomes statistically invariable with an increase in duration of observations. It is an indicative of quasi-stationarity of the seismic-energy structure which confirms stable energy state conservation of regional seismogenesis as a whole. At the same time, the second localization zone of γ is present on the diagram, where the system is introduced through a "jump" after realization of strong earthquakes (a big circle labeled as "1967", $\gamma \approx -0.470 \pm 0.015$) and over time it has been withdrawn from this segment. The attractor is likely to be more consistent with the long-term distribution of strong earthquakes; and this value should be used to estimate recurrent intervals and the probability of strong earthquakes by means of the

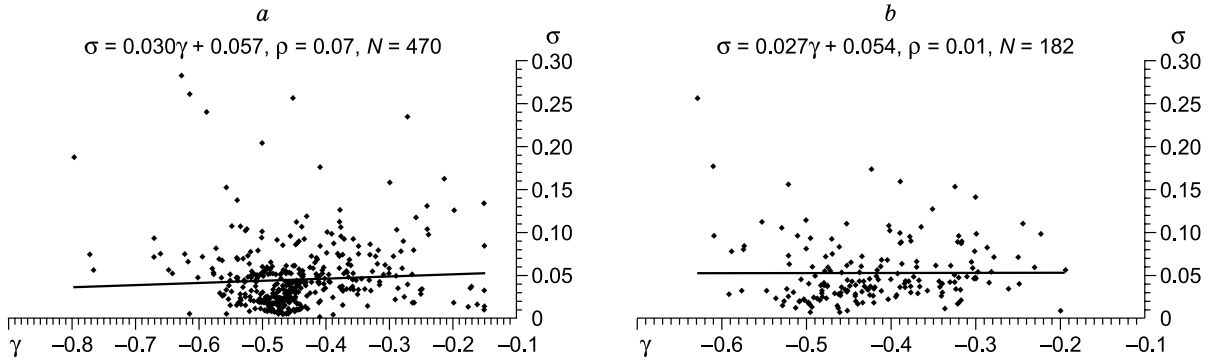

Fig. 9. Correlation of σ and γ over 470 time samples (*a*) and 182 space/area samples (*b*).

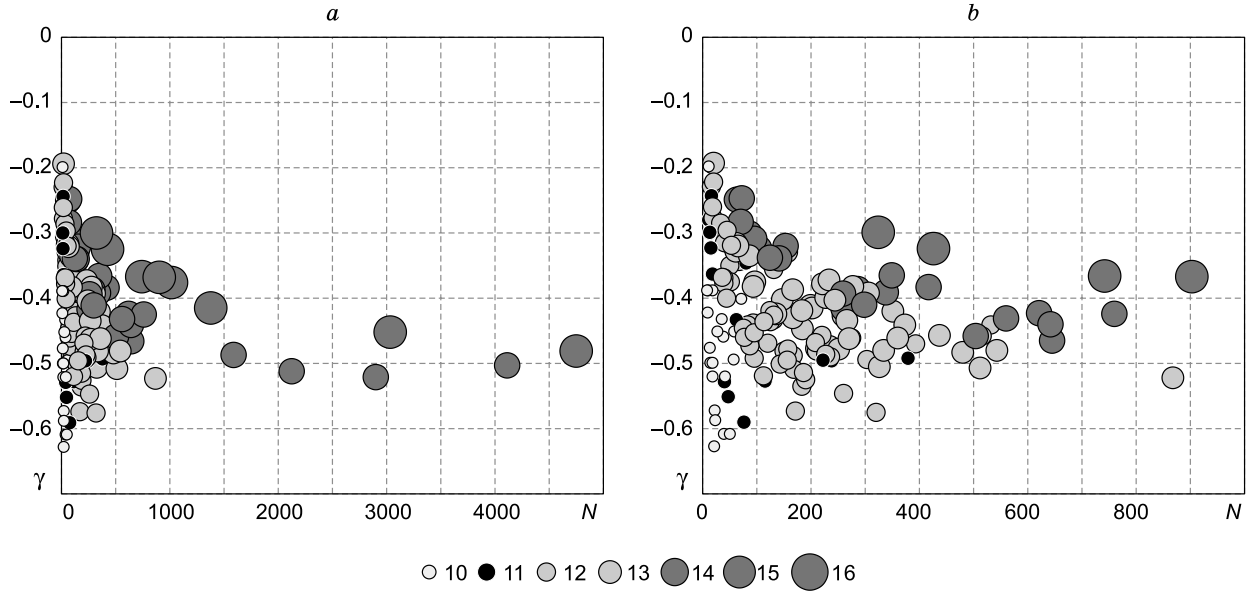

Fig. 10. The relation of γ with the number of shocks N and the value of maximum energy class K_{max} of earthquakes happening on 1° × 1° sites. *a*, over all available data samples, *b,* over samples $N \le 1000$.

γ-parameter. Note that recurrent intervals and strong earthquakes probabilities are considered to be a framework for construction the maps of general seismic zoning, where the choice of γ value is of primary importance.

According to (Andronov et al., 1981), the limiting cycle is an isolated closed trajectory in in the phase space of a dynamic system, which represents a periodic motion. In neighborhood of the limiting cycle, the phase trajectories either move away from it (unstable cycle) or come arbitrarily close to it (stable cycle). Simple analytical methods are not available either for finding the limiting cycles or for studying equilibrium positions (stationary points) and analyzing their stability. However, the study of the system phase portrait allows finding the answer to the question about the presence or absence of the limiting cycle in this system. The singularities of two attractors allocation on the phase diagram (Fig. 11) suggest that the second solution for bifurcation of the cycle origin (Andronov–Hopf bifurcation, where $\alpha > 0$), will be mostly suitable for its description. According to the theory of dynamic systems, the Andronov–Hopf bifurcation tends to arise in the typical one-parameter families and appears to be local bifurcation of the vector field in the plane, in course of which the critical point-focus loses its stability under transition of a pair of its complex-conjugate proper values through an imaginary axis. Whereby, either a short stable limiting cycle originates from a critical point (mild loss of stability, supercritical Andronov–Hopf bifurcation), or a short stable limiting cycle collapses to this point (stiff loss of stability, subcritical Andronov–Hopf bifurcation). A set of equations takes the following form in polar coordinates for the Andronov–Hopf bifurcation:

$$\begin{cases} r'(t) = r\left(\alpha - r^2\right), \\ \varphi'(t) = 1. \end{cases} \tag{5}$$

Solution (5) indicates that the dynamic system can have only one equilibrium position, which appears to be a stable focus if $\alpha \le 0$. The second solution ($\alpha > 0$) implies that the

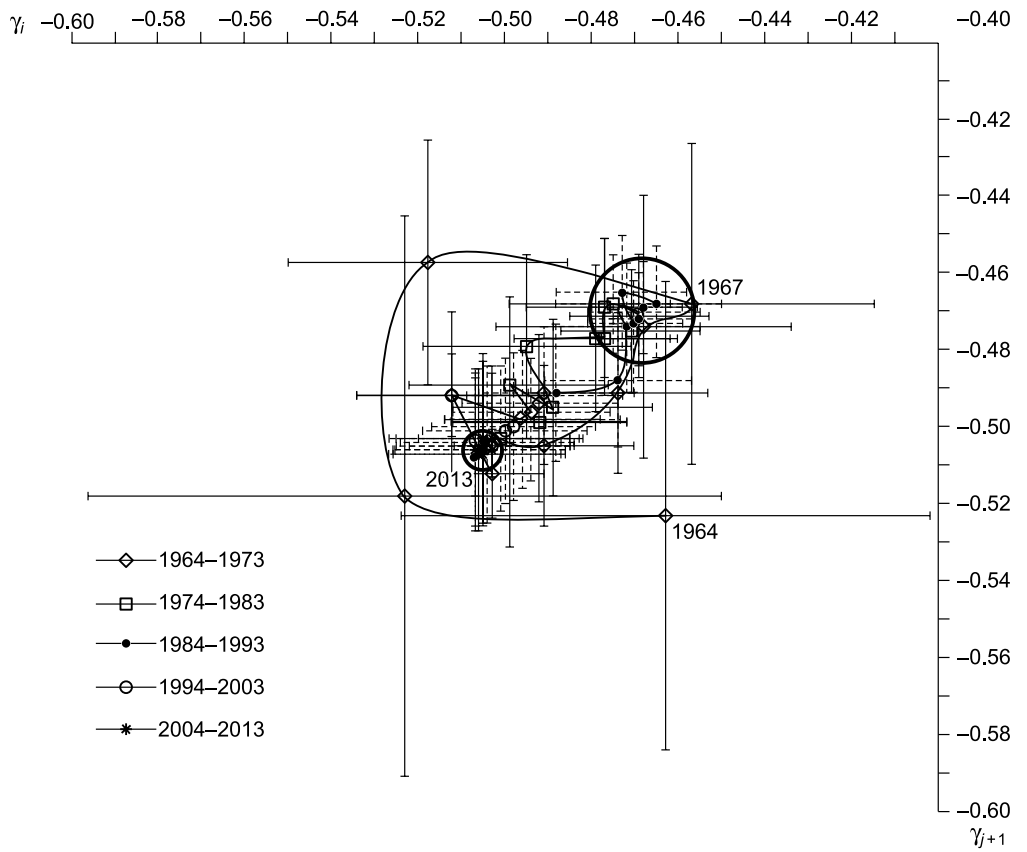

Fig. 11. The phase diagram of γ earthquakes parameter on the southwestern flank of the Baikal rift system. At the beginning the trajectory is labeled with "1967"; a circle with "1967" points at the position of the attractor basin ("unstable focus"); a circle labeled with "2013" designates the position of the attractor basin ("limiting cycle") and the end of the phase trajectory.

dynamic system can have only one equilibrium position, which appears to be an unstable focus (Fig. 11, $\gamma \approx -0.470 \pm 0.015$), and a stable limiting cycle ($\gamma \approx -0.505 \pm 0.02$). The terms of "mild" and "stiff" losses of stability relate to the system behavior description from the point of view of an external observer under conditions of slow (compared with the system dynamics) evolution of the system parameter (α) and the system noise contamination with negligible random perturbations. In case of mild loss of stability, the solution will make a transition from the equilibrium position (which becomes unstable) to the limiting cycle: an external observer will notice periodical "trembling" of the system state in vicinity of the equilibrium position, which will grow with an increase of the parameter. In case of stiff loss of stability, the solution skips suddenly and shifts to the position beyond the boundary of the repulsion basin for the disappeared limiting cycle: from the point of view of an external observer the solution has changed the setting by a leap. Presence of two γ-parameter attractors, generation of the limiting cycle from unstable focus, jump-like transition from the limiting cycle to unstable focus under realization of strong earthquakes and gradual transition from focus-point to the limiting cycle are the indicatives of close conformity of seismic-energy structure behavior on the BRS southwestern flank (Fig. 11) with the Andronov–Hopf bifurcation model, where $\alpha > 0$.

To study the cyclic instability of the γ-parameter, two simple scenarios of seismic process development were modeled in correspondence with mild and stiff losses of stability. The initial selection of 13 earthquakes was obtained with distribution by classes in the form: $n_8 = 9$, $n_9 = 3$, $n_{10} = 1$, $\gamma_p \approx -0.477$, $\rho = 1.0$. This sample reflects a stable energy state where within the whole range of energy classes, one earthquake of the next energy level (marked as the "right" lg$N$ distribution over K_R) falls at three earthquakes of each class. We call this state as the first "equilibrium", because all lg$N$ points lie on the curve and there are no moments causing a pivoted shift of the earthquake recurrence rate curve, i.e., the equilibrium exists in distribution between strong and weak earthquakes, and standard deviation $\sigma = 0$. According to the first scenario, seismicity is "smoothly" withdrawn from this stable energy state by three earthquakes, starting from the minimum class. A gradual increase of the γ trembling is observed during the earthquakes whose energy class is one unit higher the center of classes distribution; and return to the stable state of the limiting cycle occurs under realization of the shock with maximum class. The sample of the second equilibrium tends to form at the

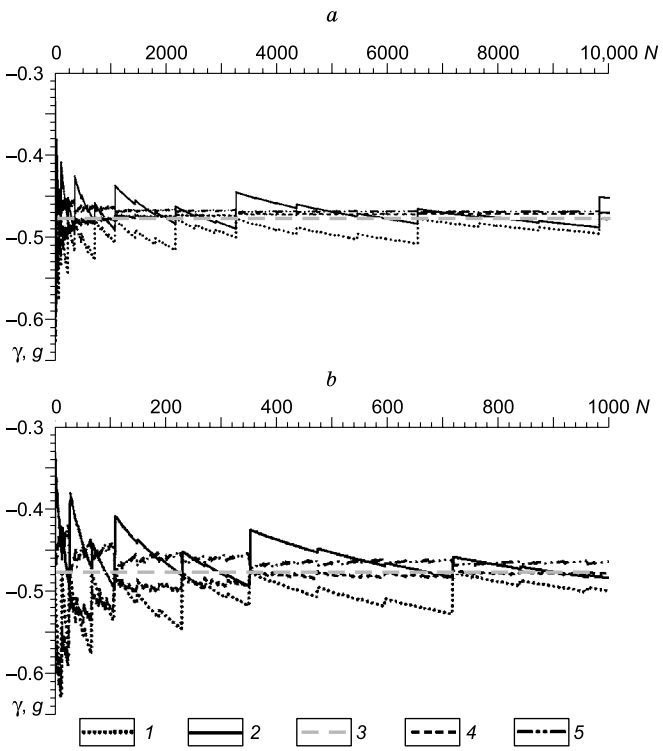

Fig. 12. Variations of the slopes on the curves γ (model 1 and model 2) and *g* (model 1 MML and model 2 MML) for "swarming" (model 1) and "aftershock" (model 2) sequences of shocks. The graphs are plotted against ten thousand (*a*) and one thousand (*b*) events. γ = –0.477 in the "equilibrium" state. *1*, model 1, *2*, model 2, *3*, equilibrium, *4*, model 1 MML, *5*, model 2 MML.

end of the first cycle: $n_8 = 27$, $n_9 = 9$, $n_{10} = 3$, $n_{11} = 1$, $\gamma = \gamma_p$, $\rho = 1.0$, at the end of the second cycle: $n_8 = 81$, $n_9 = 27$, $n_{10} = 9$, $n_{11} = 3$, $n_{12} = 1$, $\gamma = \gamma_p$, $\rho = 1.0$, etc. According to the second "stiff" scenario, seismicity is withdrawn from the stable energy state with a jump into the basin of unstable focus by means of one "the strongest" earthquake whose energy class is a unit higher than in the initial selection ($K = 11$). Return to the stable state of the limiting cycle is fulfilled by weak earthquakes in the mode of the first sample. The sample of the second equilibrium tends to form at the end of the first cycle: $n_8 = 27$, $n_9 = 9$, $n_{10} = 3$, $n_{11} = 1$, $\gamma = \gamma_p$, $\rho = 1.0$, at the end of the second cycle: $n_8 = 81$, $n_9 = 27$, $n_{10} = 9$, $n_{11} = 3$, $n_{12} = 1$, $\gamma = \gamma_p$, $\rho = 1.0$, etc. The difference between the models lies in the mechanism of exit and return to equilibrium, which is predetermined by the physical nature of this mechanism. The first scenario reflects, in general terms, a gradual increase and stress relaxation (swarming process); the second scenario implies sudden stress relieving and gradual stress restructuring (aftershock process).

Figure 12*a* represents the model slopes of γ and *g* for several cycles of exit/return to equilibrium state per ten thousand events. Figure 12*b* shows variations in γ and *g* for one thousand events in order to provide high solvability of extremely changing starting portion of the curve. Comparison of the γ and *g* curves points at their correspondence to the form, although γ is much stronger than *g* by a variation degree. It is seen that in the field of big numbers, the behavior of model curves γ is usually similar consequently, their identification is impossible if γ_p is unknown. Nevertheless, at the beginning curve segments take different forms for a small quantity of shocks (Fig. 12*b*): according to the first scenario the slopes approach γ_p from the side of lower values and do not cross it. According to the second scenario, the slopes approach γ_p from the side of higher values and cross it. These different initial curve segments allow us to find better scenario correspondence for the dynamics of the real seismic-energy structure state along the BRS southwestern flank. The curves presented in Fig. 13*a, b* characterize time changes of γ and *g* on the investigated territories for the period of 1964–2013. Then, the 14th sampled shocks are included into distribution, γ and *g* are calculated, and the procedure is repeated for each following earthquake. Comparison of γ and *g* regional curves confirms the conclusion of numeric modeling (Zhalkovskii and Muchnaya, 1987; Demyanovich and Klyuchevskii, 2013) and the results presented in Fig. 13: estimates by MML are more stable, and stability of estimates by RMS tends to rise with an increase

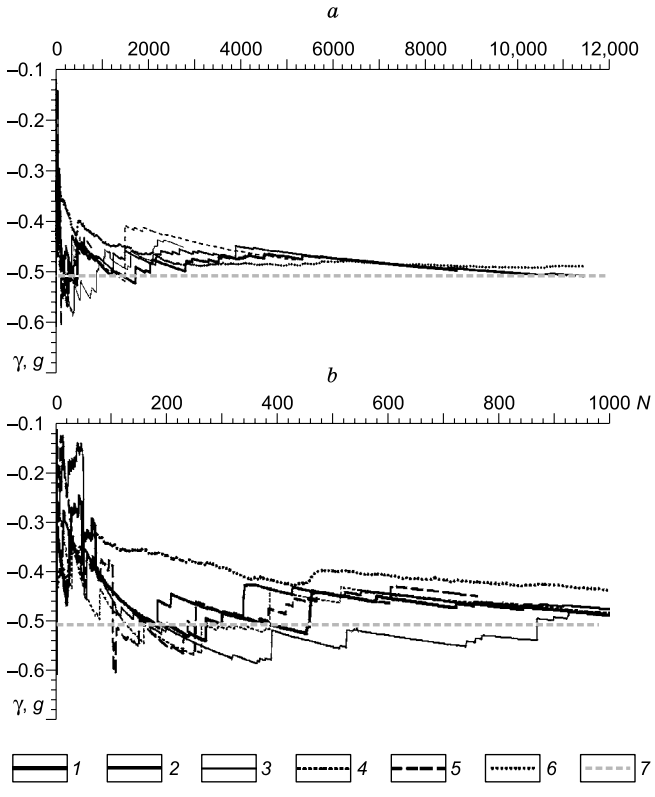

Fig. 13. Variations of the slopes on the curves γ and *g* (MML region) in the investigated territories on the southwestern flank of the BRS. The graphs are plotted for 11,442 (*a*) and one thousand (*b*) shocks. The dashed curve and the label (region 2013) represent the value γ = –0.51, that corresponds to the slope of the earthquake recurrence rate curve on the BRS southwestern flank for a period of 1964–2013. *1*, region, *2*, area 1, *3*, area 2, *4*, BB-fault, *5,* Tk-fault, *6*, MML region, *7*, region 2013.

in data volume, and g and γ are getting closer. Comparison of model and original γ, g curves (Figs. 12, 13) indicates better agreement of the second scenario with the energy state dynamics of the natural seismicity nearly on all the investigated territories (the initial curve segment of site 2 shares common traits of the first scenario). Therefore, the seismicity state dynamics on the southwestern flank of the BRS fits more the aftershock process model and it is no great surprise, because about the half of all the earthquakes account for aftershocks on this territory (Klyuchevskii et al., 2011, 2013). The main findings of the numeric modeling are consistent with real seismic-energy patterns and allow presenting more informative and justified illustration of γ instability and evaluation methods properties due to determinacy of the model events array.

DISCUSSION

Statistic regularities (Lvovskii, 1982; Aivazyan et al., 1983), are known to characterize empirical relations more precisely with an increase of data array and the range of investigated parameters. Ideally, these data arrays should be infinite or complete, but seismological practice implies the use of earthquake databases are limited in space and time. Therefore, the first shocks usually correspond to the beginning of instrumental data collection, but the sampling of the last ones depends on the availability of processed records. The sampling limitations lead to additional deviations from regulations, which are created not only by errors in determination of experimental data, but by incompleteness of the used statistic, i.e., obtained estimates are biased and depend on the sampling volume N. Since a correct statistic description of the energy structure states depends on the number of earthquakes (N) in the used sample, the obtained γ, g, A_{10} and K_{max} parameters will be more approximated to true values with an increase of N. Since a rise of N is feasible only with an increase of instrumental monitoring duration, a complete representative materials sample will be generated during a complete seismic cycle. The time span of the studies is equal to 50 years, and it is significantly shorter compared with the strong earthquake recurrence period on the southwestern flank of the Baikal Region (370 years), which is commonly characterized in terms of a seismic cycle (Klyuchevskii et al., 2005). Since the states of the seismic-energy structure are defined for a short time interval, the estimates obtained in the study appear to be different from the long-term parameters of the actual seismic-energy structure formed for a continuous seismic process period of 1000 years.

The present state dynamics study of the seismic-energy structure on the BRS southwestern flank complies with statistic regularities, and the state estimates are maximally approximated to long-term parameters and obtained over a complete selection of regional earthquakes for the time interval of 1964–2013: $\gamma \approx -0.51$, $g \approx -0.49$, $A_{10} \approx 0.05$ and $K_{max} = 16.2$ (Table 1). Deviations (sometimes rather big) from these values are observed at all levels of the spatial-time organization structure of seismicity. Annual estimates on the slopes of earthquake recurrence curves vary from $\gamma \approx -0.15$ to $\gamma \approx -0.80$, from $g \approx -0.26$ to $g \approx -0.76$; they fall in the range for seismic activity from $A_{10} \approx 0.01$ to $A_{10} = 9.6$, and for maximum energy class from $K_{max} = 9$ to $K_{max} = 16.2$. In accordance with the data on 1° × 1° sites the slopes tend to vary in the range of $0.63 \le \gamma \le -0.19$ and $-0.84 \le g \le -0.35$, seismic activity—$0.01 \le A_{10} \le 0.89$, and maximum energy class—$10 \le K_{max} \le 16.2$. Statistical annual average values obtained over the region, in two areas, in the BB- and Tk-fault zones, on 1° × 1°sites of the earthquake recurrence rate curves demonstrate (Table 2) their difference from long-term statistics. Rapid and considerable spatial-time changes of parameters are caused by realization of strong earthquakes followed by series of aftershocks, but some additional fluctuations are also due to small volumes of sampled data. The results obtained by accumulated selected data are certain to be convincing indicators of this fact since the slopes of earthquake recurrence curves in the investigated

Table 2. The average annual and average areal parameters of the earthquake recurrence curves and their standard deviations

Territory	Incline				Activity		Maximum class	
	γ	σ_γ	g	σ_g	A_{10}	σ_A	K_{max}	σ_K
	Average annual							
R	–0.44	0.07	–0.48	0.05	0.06	0.07	12.5	1.1
A1	–0.42	0.10	–0.48	0.06	0.10	0.13	12.0	1.4
A2	–0.41	0.12	–0.48	0.07	0.03	0.01	11.6	1.2
BB	–0.47	0.11	–0.52	0.08	0.91	1.79	11.5	1.4
Tk	–0.34	0.14	–0.47	0.11	0.22	0.09	10.2	1.1
	Average areal (in 1° × 1° sites)							
R	–0.42	0.09			0.06	0.11	12.5	1.4

Note. σ_γ, σ_g, σ_A, and σ_K, standard deviations of the slope of the recurrence curves (RMS, MML), seismic activity, and the maximum energy class of earthquakes.

territories differentiate significantly for the first ten years with the use of small data volumes. However, in due time, they tend to approach γ and *g* of the region and stabilize around this value (Fig. 5). The observed trend towards parameters stabilization and a decrease in their spatial-time fluctuations due to an increase of data volumes agrees well with common views on stationarity of open dynamic systems. It is known (Chereshnev, 2006) that different kinds of processes take place inside the open stationary systems participating in energy exchange with the environment, but their average parameters change slightly in the definite time interval though they stay unchanged in various parts of the system. The methods of statistical analysis illustrate the stationarity of the seismic mode (population of earthquakes being studied in time and space) (Gaiskii, 1970), so a phenomenological model of a stationary seismic process has been developed, where seismic activity of the lithosphere is considered to be a sum total of small spatial-time fluctuations of the evolutionary planet process (Sadovskii et al., 1987). The analysis of the seismic process energetics on the assumption of its stationarity is based on the fact that "…the sources of the tectonic process energy, which engender seismicity, appear to be inexhaustible for a certain period of time; and a part of the tectonic process energy participating in seismicity, including the potential energy of the imminent earthquake sources, remains constant on an average for the whole process period" (Riznichenko, 1968, p. 18). Polyperiodicity of the Earth's geological history gives evidence in favor of tectonic processes nonstationarity. Based only on the fact that they change in time very slowly, steady-state approximation is admitted by the analyses of the present time seismicity (at least the Holocene). The steady-state approximation allows correct seismic zoning and evaluation of seismic territorial hazards by the analysis of spatial-time variations in the seismic-energy structure of different hierarchical levels in relation to parameters of the long-term seismogenesis. However, the lower time limit should correspond to the seismic cycle of the investigated territory, because it is the only case when the structures of natural and recorded seismicity will be identical to each other.

Knowledge and consideration of fundamental laws of nonlinear nature allow us to improve our understanding of the system dynamics and predict its behavioral characteristics in bifurcations when it changes its trajectory, commonly in a disastrous way. Understanding of seismic-energy structure dynamics to the extent of the Andronov–Hopf bifurcation leads to necessity of considering important theoretical and application problems in the field of seismic intensity. The presence of two attractors in the dynamics of the seismic-energy system structure raises the question which attractor should be considered for general seismic zoning. Since the limiting cycle represents a stationary mode with the definite amplitude which does not depend on the starting conditions, the condition of ergodicity will be met in the dynamic system. A.T. Winfree (1980) called the domains where two modes/settings are possible (focus and the limiting cycle) a black hole. According to him, in this parameter domain the excitation could be as applied to the oscillating system, that it will get into the domain of the rest point attraction, thus it will result in vibration damping. In particular, it is illustrated for equations modeling the behavior of the first pulse (Riznichenko, 2011). In relation with the results obtained, it may indicate the probability of the seismic process realization without disastrous earthquakes under certain conditions.

CONCLUSIONS

To study the state dynamics of the seismic-energy structure on the southwestern flank of the BRS, the statistical-analysis has been performed for the parameters of the earthquake recurrence curves with $K_R \geq 8$ for a period of 1964–2013. It has been found that the most significant variations of maximum energy class K_{max}, the slopes of γ and *g* recurrence curves and seismic activity A_{10} occur in presence of strong earthquakes. We evaluated the dependence on the ways of the parameters calculation and the *N* volumes of sampling estimation. The variation of estimates has been shown to decrease at *N* exceeding one thousand events. Consequently, the determination of parameters for earthquake recurrence curves becomes stable for this quantity of shocks; and standard deviation from γ tends to decrease by power law. The observed trend towards parameters stabilization and a decrease in their spatial-time fluctuations due to an increase of data volumes agrees well with the common views on the stationarity of open dynamic systems. The presence of two γ-parameter attractors, a jump-like transition from one attractor (the limiting cycle) to another (unstable focus) under realization of strong earthquakes and gradual transition from the focus-point to the limiting cycle are the indicatives of close conformity of seismic-energy structure behavior on the BRS southwestern flank with the Andronov–Hopf bifurcation model. To study the characteristics and process formation specifics, calculations of γ and *g* were done, where they characterize the state dynamics of the seismic-energy structure in the scenarios of "aftershock" and "swarming" series of shocks. Comparison of model and original variations of γ and *g* curves indicates better agreement of the aftershock model with the energy state dynamics of the natural seismicity in all the investigated territories on the southwestern flank of the BRS.

The research was partially supported by the RFBR (14–05–00308_a, 14–45–04011_ p_Sibir'_a).

REFERENCES

Aivazyan, S.A., Enyukov, I.S., Meshalkin, L.D., 1983. Applied Statistics [in Russian]. Finansy i Statistika, Moscow.

Andronov, A.A., Vitt, A.A., Khaikin, S.E., 1981. The Theory of Vibrations [in Russian]. Nauka, Moscow.

Chereshnev, V.A. (Ed.), Human Ecology in the Changing World [in Russian]. UrO RAN, Yekaterinburg.

Dem'yanovich, V.M., Klyuchevskii, A.V., Chernykh, E.N., 2008. Lithospheric stress and strain and the seismicity in the Belin-Busiingol fault zone, southern Baikal region. J. Volcanol. Seismol. 2 (1), 40–54.

Demyanovich, V.M., Klyuchevskii, A.V., 2013. Comparative analysis of parameters of earthquake recurrence rate curves over given shocks distribution, in: Geodynamic Lithosphere Evolution of the Central Asian Mobile Belt (from the Ocean to the Continent), Vol. 11 [in Russian]. IZK SO RAN, Irkutsk, pp. 87–88.

Doser, D.I., 1991. Faulting within the western Baikal rift as characterized by earthquake studies. Tectonophysics 196, 87–107.

Dzhurik, V.I., Klyuchevskii, A.V., Serebrennikov, S.P., Demyanovich, V.M., Batsaikhan, Ts., Bayaraa, G., 2009. Seismicity and Zoning of Seismic Hazards on the Territory of Mongolia [in Russian]. IZK SO RAN, Irkutsk.

Earthquakes of Russia in 2005, 2007 [in Russian]. GS RAN, Obninsk.

Earthquakes of Northern Eurasia, 2010 [in Russian]. GS RAN, Obninsk.

Gaiskii, V.N., 1970. Statistical Investigations of the Seismic Setting [in Russian]. Nauka, Moscow.

Golenetskii, S.I., 1981. Towards justification of the earthquake summation method for quantitative seismicity estimation, in: Seismic Investigations in Eastern Siberia [in Russian]. Nauka, Moscow, pp. 54–62.

Golenetskii, S.I., 1989. Earthquakes of the Baikal Region and Transbaikalia, in: Earthquakes of the USSR [in Russian]. Nauka, Moscow, pp. 112–122.

Golenetsky, S.I., 1990. Problems of seismicity of the Baikal rift zone. J. Geodynamics 11, 293–307.

Golenetskii, S.I., Demyanovich, V.M., Filina, A.G., 1993. Representativeness of earthquakes in Southern Siberia and Mongolia from 1980 to1990, in: Seismicity and Seismic Zoning of Northern Eurasia, Vol. 1 [in Russian]. Moscow, pp. 83–85.

Gor'kavyi, N.N., Levitsky, L.S., Taidakova, T.A., Trapeznikov, Yu.A., Fridman, A.M., 1999. On dependence of correlation between regional Earth seismicity and irregularities of the Earth rotation on depths of earthquake sources. Fizika Zemli, No. 11, 52–66.

Keilis-Borok, V.I., Knopoff, L., Rotwain, I., Allen, C.R., 1988. Intermediate term prediction of occurrence times of strong earthquakes. Nature 335 (6192), 690–694.

Klyuchevskii, A.V., 2005. earthquake scales of the Baikal Region. Vulkanologiya i Seismologiya, No. 3, 51–61.

Klyuchevskii, A.V., 2007. Stresses and seismicity at the present stage of evolution of the Baikal rift zone lithosphere. Izvestiya. Phys. Solid Earth 43 (12), 992–1004.

Klyuchevskii, A.V., 2010. Nonlinear geodynamics of the Baikal Rift System: an evolution scenario with triple equilibrium bifurcation. J. Geodyn. 49 (1), 19–23.

Klyuchevskii, A.V., 2011. Attractor structures of riftogenesis in the lithosphere of Baikal Rift System. Dokl. Earth Sci. 437 (1), 407–411.

Klyuchevskii, A.V., 2014. Rifting attractor structures in the Baikal Rift system: location and effects. J. Asian Earth Sci. 88, 246–256.

Klyuchevskii, A.V., Dem'yanovich, V.M., 2003. Correspondence between spatiotemporal variations in geodynamic and seismic processes in the Baikal region. Dokl. Earth Sci. 390 (4), 615–619.

Klyuchevskii, A.V., Demyanovich, V.M., 2004. Seismicity of the fault zones of the Southern Baikal Region, in: Town: Past, Present, Future [in Russian]. Irkusk. Gos. Tekh. Univ., Irkutsk, pp. 77–81.

Klyuchevskii, A.V., Dem'yanovich, V.M., 2006. Stress-strain state of the lithosphere in the southern Baikal region and northern Mongolia from data on seismic moments of earthquakes. Izvestiya. Phys. Solid Earth 42 (5), 416–428.

Klyuchevskii, A.V., Klyuchevskaya, A.A., 2009. Seismic process in the lithosphere of the Baikal Rift Zone: Synchronization episodes. Dokl. Earth Sci. 425 (1), 340–344.

Klyuchevskii, A.V., Khlebopros, R.G., 2013. Coupled large earthquakes in the Baikal rift system: Response to bifurcations in nonlinear resonance hysteresis. Geosci. Front. 6, (4), 709–716.

Klyuchevskii, A.V., Zuev, F.L., 2007. Structure of the epicenter field of earthquakes in the Baikal region. Dokl. Earth Sci. 415 (2), 944–949.

Klyuchevskii, A.V., Dem'yanovich, V.M., Dzhurik, V.I., 2009. Hierarchy of earthquakes in the Baikal rift system: implications for lithospheric stress. Russian Geology and Geophysics (Geologiya i Geofizika) 50 (3), 279–288.

Klyuchevskii, A.V., Demyanovich, V.M., Klyuchevskaya, A.A., 2011. earthquake groups of the Baikal rift zone: statistics and spatial-time distribution, in: Geodynamic Lithosphere Evolution of the Central Asian Mobile Belt (from the Ocean to the Continent), Vol. 9 [in Russian]. IZK SO RAN, Irkutsk, pp. 99–101.

Klyuchevskii, A.V., Demyanovich, V.M., Klyuchevskaya, A.A., 2012. Uncertainties of parameters evaluation of earthquake recurrence rate curves in the Baikal Region, in: Contemporary Geodynamics of Central Asia and Natural Hazardous Processes: Research Findings on the Quantitative Basis, Vol. 2 [in Russian]. IZK SO RAN, Irkutsk, pp. 33–36.

Klyuchevskii, A.V., Dem'yanovich, V.M., Dzhurik, V.I., 2013. Estimating the energy of seismotectonic deformations in the lithosphere of the Baikal Rift Zone. J. Volcanol. Seismol. 7 (4), 277–292.

Klyuchevskii, A.V., Dem'yanovich, V.M., Klyuchevskaya, A.A., 2015. Energy structure of seismicity at the southwestern flank of the Baikal rift system. Dokl. Earth Sci. 464 (2), 1069–1074.

Logachev, N.A., 2003. History and Geodynamics of the Baikal Rift. Geologiya i Geofizika (Russian Geology and Geophysics) 391–406 (373–388).

Lvovskii, E.N., 1982. Statistical Methods of Empirical Equations Formulation [in Russian]. Vysshaya Shkola, Moscow.

Malinetskii, G.G., Potapov, A.B., 2000. Modern Problems of Nonlinear Dynamics [in Russian]. URSS, Moscow.

Nikolis, G., Prigozhin, I., 2003. Cognition of Complexity [in Russian]. URSS, Moscow.

Prigozhin, I., Stengers, I., 1985. Order from Chaos [in Russian]. Progress, Moscow.

Rautian, T.G., 1964. On seismic-energy determination at a distance up to 3000 km. Eksperimental'naya Seismika. Trudy IZK AN SSSR 32 (193), 86–93.

Riznichenko, G.Yu., 2011. Lectures on mathematical models in biology [in Russian]. SRC Regular and Chaotic Dynamics, Moscow–Izhevsk.

Riznichenko, Yu.V., 1964. The Method of earthquake summation for studying seismic activity. Izvestiya AN USSR. Geophys. Ser., No. 7, 969–977.

Riznichenko, Yu.V., 1968. The energy model of the seismic setting. Izvestiya AN USSR. Fizika Zemli, No. 5, 3–19.

Riznichenko, Yu.V., Artamonov, A.M., 1975. Energy model development for spatial-time seismic-energy distribution. Izvestiya AN USSR. Fizika Zemli, No. 12, 35–42.

Ruzhich, V.V., Levina, E.A., Pisarenko, V.F., Lyubushin, A.A., 1998. Statistic estimation of the maximum possible earthquake magnitude for the Baikal Rift Zone. 39 (10), 1443–1455 (1445–1457).

Sadovskii, M.A., 1979. Natural granulometric rock composition. Dokl. Akfd. Nauk SSSR 247 (4), 829–831.

Sadovskii, M.A., Bolkhovitinov, L.G., Pisarenko, V.F., 1987. Deformation of the Geophysical Medium and the Seismic Process [in Russian]. Nauka, Moscow.

Sobolev, G.A., 1999. Preparation stages of strong Kamchatka earthquakes. Vulkanologiya i Seismologiya, Nos. 4–5, 63–72.

Stepin, V.S. (Ed.), 2010. New Encyclopedia of Philosophy [in Russian]. Mysl', Moscow, Vol. 3.

Sykes, L.R., Jaume, S.C., 1990. Seismic activity on neighboring faults as a long-term precursor to large earthquakes in the San Francisco Bay area. Nature 348 (6302), 595–599.

Wiemer, S., Wyss, M., 1994. Seismic quiescence before the Landers (M = 7.5) and Big Bear (M = 6.5) 1992 earthquakes. Bull. Seismol. Soc. Am. 84 (3), 900–916.

Winfree, A.T., 1980. The Geometry of Biological Time. Springer-Verlag, New York–Heidelberg–Berlin.

Zav'yalov, A.D., 2006. Medium-Term earthquake Forecast: Fundamentals, Methodology, Realization [in Russian]. Nauka, Moscow.

Zhalkovskii, N.D., Muchnaya, V.I., 1987. Accuracy of determining the slope of the graph of earthquake frequency. Geologiya i Geofizika (Soviet Geology and Geophysics) 114–120 (103–109).

Editorial responsibility: V.S. Seleznev